Tribology International 41 (2008) 985–991

Contents lists available at ScienceDirect

Tribology International

journal homepage: www.elsevier.com/locate/triboint

Microstructural and tribological study of Nd:YAG laser treated titanium plates

M.C. Marco de Lucas *, L. Lavisse, G. Pillon

Institut Carnot de Bourgogne, UMR 5209 CNRS-Université de Bourgogne, 9 Av. A. Savary, BP 47 870, F-21078 DIJON Cedex, France

ARTICLE INFO

Article history:
Received 31 August 2007
Received in revised form
4 March 2008
Accepted 11 March 2008
Available online 15 May 2008

Keywords:
Fretting
Laser treatments
Raman spectroscopy
Titanium oxides

ABSTRACT

In this work, the fretting behaviour of pure Ti plates laser treated with a Nd:YAG pulsed laser was compared to that of untreated Ti plates. Fretting tests were done at room temperature without lubrication. The contact geometry was a cylinder (bearing steel) on a plane. The evolution of both the ratio, $\mu = Q/P$, between the normal and the tangential forces, and the Fouvry's energy criterion (A) were recorded as a function of the number of fretting cycles, N. Energy dispersive spectrometry and micro-Raman spectroscopy were used to analyse the fretting scars. The oxidized layer formed by the laser treatment displayed a mixed slip regime as a function of N, and a smaller fretting coefficient μ than the titanium reference.

1. Introduction

Titanium and its alloys have a wide range of applications in the fields of chemical industry, aerospace, marine and biomedical devices because of their combination of properties in terms of high strength to weight ratio, exceptional resistance to corrosion and excellent biocompatibility. The native oxide layer grown on the Ti surface is at the origin of the excellent corrosion resistance of titanium because of its chemical stability and adherence. However, titanium shows poor tribological properties, which include highly unstable friction coefficients and low wear rate [1,2]. In order to overcome this problem, different surface treatments can be used producing a surface layer with good tribological properties. Thermal oxidation, anodizing, oxygen diffusion, and ion implantation are some of the most common methods used to produce a thick oxide layer on the Ti surface [3–6]. Among them, thermal oxidation is relatively simply done and produces thick, highly crystalline oxide films. However, titanium dioxide microstructure and stoichiometry are sensitive to the annealing conditions in terms of annealing temperature and cooling rate [1]. The rutile phase is the most stable TiO_2 phase but other phases such as anatase, brookite and the sub-stoechiometric Ti_nO_{2n-1} Magneli phases can also be obtained. The interesting tribological properties of titania-based Magneli phases have been reported by Storz [7] and Woydt [8].

Laser surface treatments, thanks to their specific thermal characteristics, allow one to obtain surface layers with unsual microstructures [9–11] which can show potentially interesting tribological properties. In this work, the surface of Ti substrates was irradiated by a Nd:YAG pulsed Q-switched laser ($\lambda = 1.064\,\mu m$) in order to produce a thick oxide layer at the surface of the Ti substrate with a limited deformation of the surface. Then, fretting tests were done in order to study the tribological behaviour of the laser treated surface. Previous works [10,12,13] reported morphological and structural studies of the formed layers as a function of the laser fluence in the 4–60 $J\,cm^{-2}$ range. The present works deal with the fretting behaviour of blue layers obtained with laser fluence values about 35 $J\,cm^{-2}$. Scanning electron microscopy (SEM), energy dispersive spectrometry (EDS) and micro-Raman spectroscopy are used to study the modification of the surface layer in the fretting scars.

2. Experimental details

2.1. Laser treatment of the Ti plates

Commercially pure titanium (grade 4) plates of dimensions 15 mm × 10 mm × 1.2 mm were used. Prior to laser treatment, the sample surfaces were mechanically polished with 1200-grit SiC before an electrolytic polishing in a perchloric acid with ethylene glycol in methanol solution for 30 s at 24 V and 2 A to obtain a reference surface with very low roughness ($Ra < 0.4\,\mu m$). Previous SEM observations revealed no features on such prepared samples

* Corresponding author.
E-mail address: delucas@u-bourgogne.fr (M.C. Marco de Lucas).

0301-679X/$ - see front matter © 2008 Elsevier Ltd. All rights reserved.
doi:10.1016/j.triboint.2008.03.007

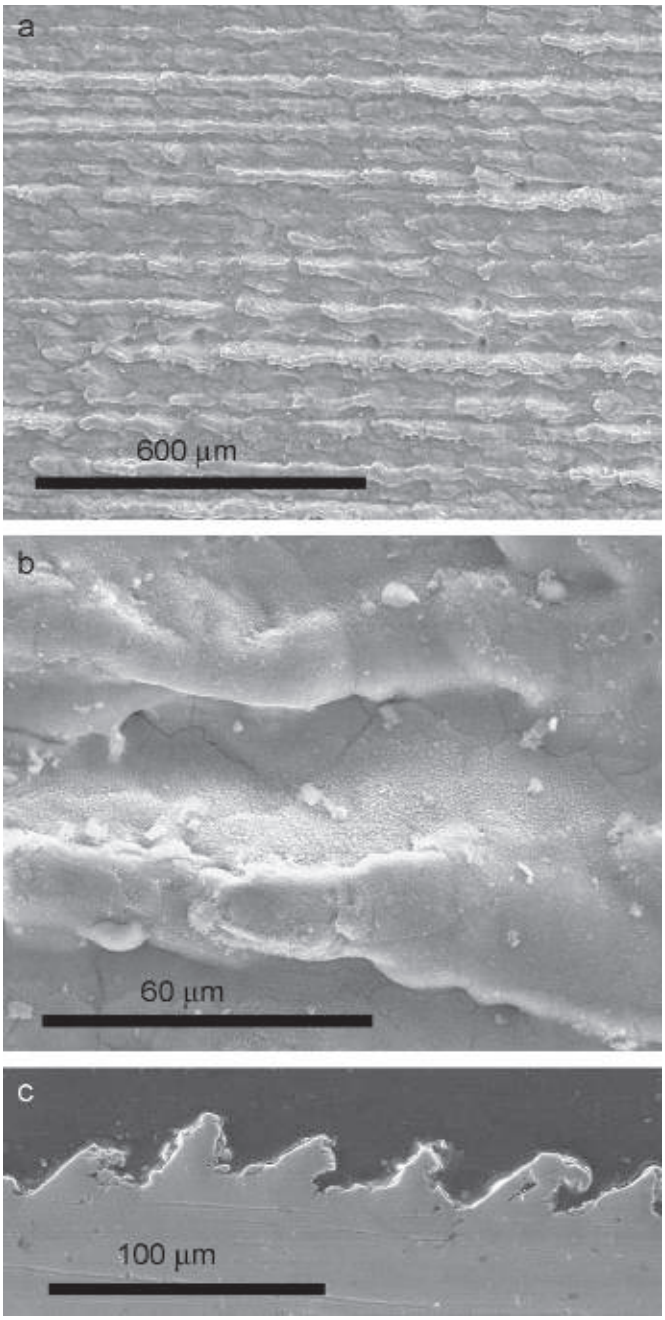

Fig. 1. (a,b) SEM top view of the layer formed at the surface of a Ti substrate by pulsed laser treatment, (c) cross-sectional view.

[12]. XPS analysis showed the formation of a very thin layer of titanium dioxide at the surface of the samples.

The laser treatments were performed in air using a Nd:YAG Q-switched laser with a wavelength of 1.064 μm, a pulse duration of 35 ns and a repetition rate $f = 5$ kHz. The average laser power has been measured after standardizing with a Coherent 200XL calorimeter. The focused laser spot, with a diameter of about 100 μm, was moved over the titanium substrate surface with a scanning speed of 50 mm s^{-1} to form parallel straight lines (Fig. 1). It is worth noting that the overlap between adjacent laser pulses must be taken into account in order to calculate the cumulative fluence on the substrate. An overlap factor around 50 can be evaluated by considering a Gaussian distribution of the laser beam energy, which leads to a circular shape spot, and a step of 40 μm between adjacent laser traces. The laser fluence per pulse, F_{1p} ($J\,cm^{-2}$), can be calculated by the equation $F_{1p} = P_l/(A \cdot f)$, P_l being the average laser power (in W), A the laser spot area (in cm^{-2}) and f the repetition rate (in s^{-1}). The laser fluence per pulse was kept about 35 $J\,cm^{-2}$. Table 1 summarizes the laser treatment conditions used in this work.

Table 1
Irradiation conditions employed for the treatment of Ti substrates with a Nd:YAG Q-switched laser

Mode	f (kHz)	d (ns)	P_l (W)	F_{1p} ($J\,cm^{-2}$)	I_{1p} ($GW\,cm^{-2}$)	d (m)	v ($m\,s^{-1}$)
TEM 02	5	35	14	35	1.0	0.200	0.050

Mode, laser mode; f, laser repetition rate; d, pulse duration; P_l (W), average laser power; F_{1p} ($J\,cm^{-2}$), fluence per pulse; I_{1p}, irradiance; d, focusing distance (m); v ($m\,s^{-1}$), scanning speed.

The layers obtained with these irradiation conditions are around 50 μm thick and they display good adherence to the Ti substrate. The layers color is blue and their surface displays a *plowed field* aspect (Fig. 1). The grooves correspond to the passage of the laser beam. Between two adjacent grooves, the matter laterally pushed away by the laser beam looks like the crest of a wave. The 3D roughness parameters are approximately Sa = 6.1 μm and Sq = 9.0 μm. The chemical and structural study of these layers was reported in [12,13]. Titanium dioxide together with titanium sub-oxides were found. The anatase phase of TiO_2, with a smaller quantity of the rutile phase, was mainly found in the crests between two adjacent grooves.

2.2. Fretting details

Fretting tests were done at room temperature without lubrication with an alternative fretting device based on an electromagnetic exciter [14]. The contact geometry was a cylinder on a plane. The cylinder was made of bearing steel (100Cr6 steel, hardness HRC 60). The cylinder diameter was 20 mm and the lateral width was 2.66 mm (Fig.2). The cylinder geometrical profile was characterized before fretting tests within a profilometer (Fig. 2). It shows 1 and 2 μm high bumps at the extremities of the cylinder which are due to the machining process. It is worth noting that these defects in the cylinder profile are quite smaller than the sample surface roughness and the oxide layer thickness.

The Ti plates were rubbered to a steel bulk. The cylinder was subjected to alternating movement with an amplitude $\delta = \pm 300$ μm and a frequency of 20 Hz. The cylinder movement direction was perpendicular to that of laser scanning in the irradiated samples. The normal force on the cylinder was kept to 18 ± 2 N leading to a contact pressure of 120 ± 10 MPa. Fretting tests were done with a finite number of cycles varying from 5×10^3 to 3×10^4 cycles. The measured values of the normal force, P, the tangential force, Q, and the displacement amplitude δ were acquired and processed by an specific software.

The influence of many experimental parameters on the fretting damage has been rationalized by the introduction of fretting map concepts [15,16] which incorporate the materials and the mechanical aspect of the fretting damage [17]. Two sets of fretting maps have been proposed: the running condition fretting maps (RCFM) and the material response fretting maps (MRFM) (Fig. 3). The first one defines, as a function of the normal load and the imposed relative displacement, different fretting regimes (partial slip, mixed and gross slip regimes) which are characterized by the nature of the contact conditions (i.e. partial slip or gross slip) and its changes as a function of the number of cycles. By analogy with RCFM, the MRFM define the main initial damage (cracking,

particle detachment) for various combinations of the normal load and relative displacement [17]. Thus, the most dangerous working regimes can be avoided by modifying the normal loadings or the displacement amplitude. To delimit the transition between the partial slip and the gross slip regimes, three quantitative criteria were proposed by Fouvry [16,18,19]. One of them was the energy criterion A, defined as the ratio $A = E_d/E_t$ between the dissipated energy (fretting loop area) and the total energy of the cycle. The critical value $A_t = 0.2$ theoretically determines the transition from partial slip, for A values lower than 0.2, to gross slip for A values higher than 0.2 [16].

In this work, we analyse the evolution of both the friction pseudo-coefficient $\mu = Q/P$ and the Fouvry's energy criterion A as a function of the number of cycles, N. The depth of the Hertz maximal tangential strain was calculated to be about 25 μm taking into account the parameters characterizing the contact geometry and the mechanical properties of the involved materials (Young modulus $E = 104$ GPa, Poissons's coefficient $\nu = 0.35$). The thickness of the layer formed on the surface of the laser treated Ti plates is about two times this value.

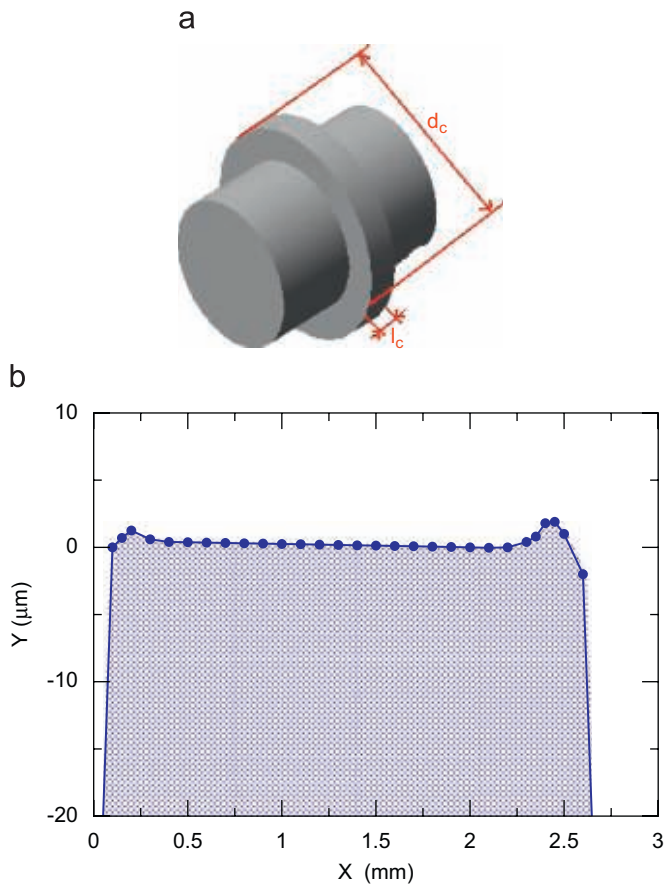

Fig. 2. (a) Scheme of the cylinder used for the fretting tests. The cylinder diameter, d_c, is 20 mm and the lateral width, l_c, is 2.66 mm. (b) Lateral profile of the cylinder.

2.3. Characterization techniques

The surface morphology of the samples was observed by SEM before and after the fretting process. The apparatus was a JEOL JSM 6400F typically working at 20 keV. X-ray analysis was performed by energy dispersive spectrometry (EDS—OXFORD—Inca energy software).

Raman spectra were obtained with a Jobin-Yvon T64000 spectrometer composed of a double subtractive pre-monochromator (stages 1 and 2) and a spectrograph stage (stage 3). The spectra were obtained in backscattering configuration. The excitation was provided by an Ar–Kr ion laser. The wavelength was 488.0 nm. Special care was taken to avoid heating the samples with the laser beam, in particular for the analysis of the fretting areas where iron oxides were found.

3. Results

3.1. Fretting results

Fig. 4 shows the variation of the ratio $\mu = Q/P$ and the energy criterion, A, as a function of the number of fretting cycles for a Ti laser treated sample, and an untreated Ti plate used as a reference. The ratio μ does not significantly change with the number of fretting cycles for both the laser treated sample and the Ti reference, but its value is almost two times lower for the laser treated sample. This result is in agreement with those reported in Ref. [1] in the case of thermal oxidation of titanium plates.

The energy criterion, A, displays different behaviours for the laser treated Ti sample and the untreated Ti reference. For this latter one, we observe almost no variation of A as a function of the number of fretting cycles, but a large dispersion of experimental

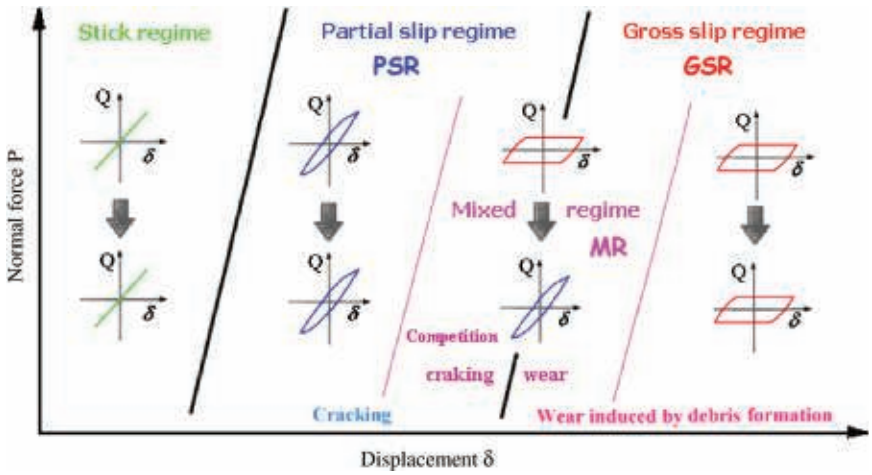

Fig. 3. Running condition fretting maps (RCFM) and material response fretting maps (MRFM) [17].

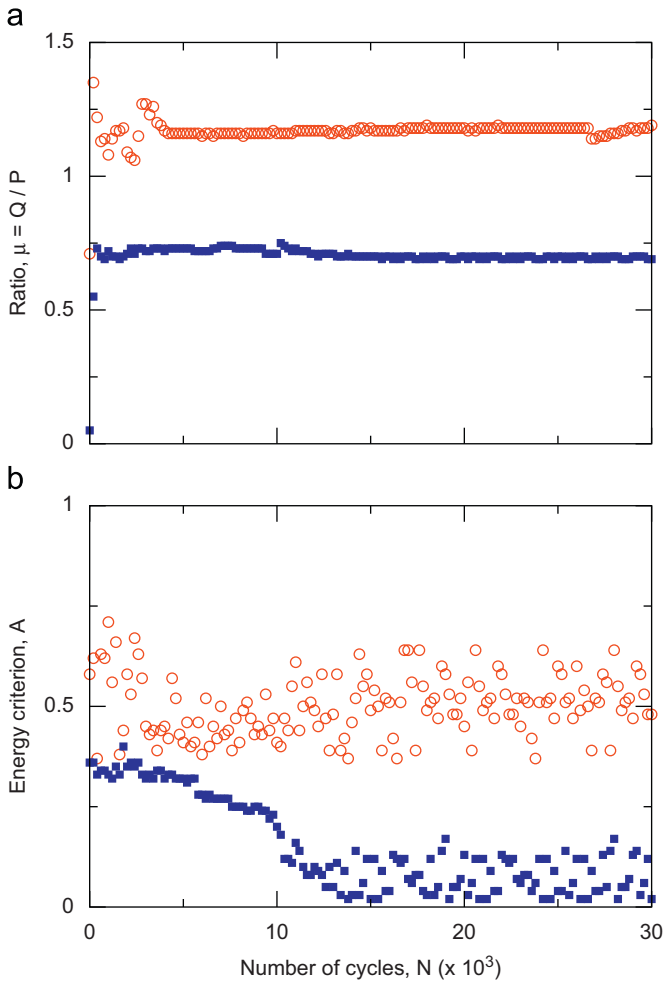

Fig. 4. Variation of (a) the ratio between the tangential and the normal forces, $\mu = Q/P$, and (b) the energy criterion, A, as a function of the number of cycles in the fretting tests. Open symbols correspond to a reference Ti sample, full symbols correspond to a laser treated Ti sample.

values around a mean value of about 0.5. Thus, the contact couple works only in gross slip regime.

For the laser treated Ti sample, the energy criterion, A, strongly varies with the number of fretting cycles. Three zones can be distinguished:

(1) For $N < 5 \times 10^3$ cycles, the energy criterion A is almost constant, about $A = 0.34$; thus, the contact couple works only in gross slip regime.
(2) For 5×10^3 cycles $< N < 1.2 \times 10^4$ cycles, A decreases continuously down to 0.2 for $N = 10^4$ cycles and abruptly it falls down to about 0.075; thus the contact changes from gross slip to partial slip regime.
(3) For $N > 1.2 \times 10^4$ cycles, A is constant, about 0.075, but a large dispersion around this value is observed, as in the case of the untreated Ti reference. The contact couple works in a partial slip regime.

3.2. Surface morphology and chemical composition

Fig. 5 shows the surface morphology of the fretting scars for a numbers of cycles varying from 5×10^3 to 3×10^4 cycles. The scars extent increases with the number of cycles as a consequence

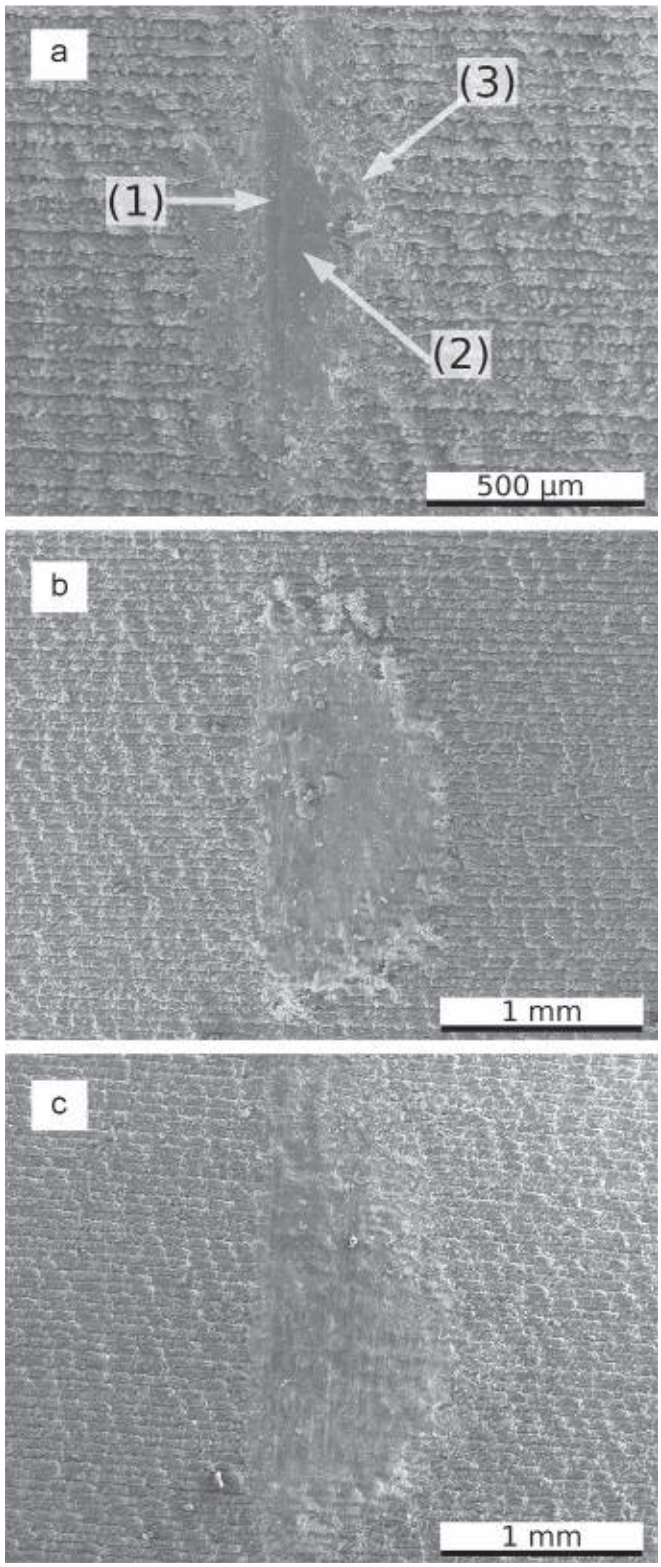

Fig. 5. SEM top views of the fretting scars in laser treated Ti samples after (a) 5×10^3 cycles, (b) 2×10^4 cycles and (c) 3×10^4 cycles. In (a), labels (1), (2) and (3) indicate, respectively, the furrow formed at the border of the contact area, the center and the periphery of the fretting scar.

of the evolution of the contact surface during the fretting process. Three main areas can be distinguished in a scar (Fig. 5a): a narrow and straight furrow, a smooth and flat area at the centre of the scar, and a rough and heterogeneous area at the periphery

Table 2
Chemical compositions (at%) obtained by EDS analysis before and after fretting tests as a function of the number of fretting cycles, N

N (cycles)	0		5×10^3			10^4			2×10^4	3×10^4
Selected region	Layer		Scars			Scars			Scars	Scars
Analysed point	Grooves	Crests	Center	Periphery		Center	Periphery		Mean	Mean
				High	Low		High	Low		
Ti	50	30	8	32	46	6	2	23	8	7
O	50	70	66	67	51	67	62	72	68	67
Fe	0	0	26	1	3	27	36	5	24	26

Before fretting tests ($N = 0$), the results obtained in the grooves and in the crests of the laser treated Ti plates are indicated. For $0 < N < 2 \times 10^4$ cycles, the composition obtained at the center and the periphery of the fretting scar are given. Moreover, high and low points are distinguished in the periphery of the scar. For $N > 2 \times 10^4$ cycles no significant differences were found between the center and the periphery of the scar, mean composition values are given.

displaying clusters of matter. The degradation of the contact surface displays a lateral evolution involving matter ejection at the contact border. The straight furrow observed in the scars is related to the border of the contact area, where shear strains concentration is induced by border effects. Moreover, the machining defects observed in both extremities of the cylinder profile (Fig. 2) increase strains concentration at the border of the contact area.

Table 2 summarizes the results obtained by EDS analysis of the samples before and after fretting tests. Before fretting tests ($N = 0$), the oxygen/titanium content decreases from the crests to the grooves in the laser treated surface. Previous works reported the microstructural study of these layers [10,12,13]. In the crests, the anatase phase of TiO_2 was mainly found together with a smaller quantity of the rutile TiO_2 phase. In the grooves, the contribution of these phases is lower while that of sub-stoechiometric titanium oxides (TiO_x) increases.

The heterogeneity of the fretting scars leads to a large interval of EDS results as a function of the analysed area and the number of fretting cycles. In the centre of the scar, the obtained composition is almost the same independently of the number of fretting cycles. A high content of iron is detected, about 26 at%, while the measured Ti content is reduced to approximately 7 at% in this region. This reveals a transfer of matter from the cylinder to the sample even for the lowest number of cycles, $N = 5 \times 10^3$.

In the periphery of the scars, the situation is more complex and it depends on the number of fretting cycles. For the lowest number of cycles, $N = 5 \times 10^3$, the results obtained by EDS vary from low to high points on the rough periphery of the scar, and they are close to those obtained, respectively, in the grooves and in the crests of the surface layer. Almost no iron (1–3 at%) was detected in this region. For $N = 10^4$ cycles, the content of iron strongly increases up to about 36 at% in the highest points of the scar periphery. For $N > 2 \times 10^4$ cycles, the roughness of the scar periphery decreases. EDS results do not change significantly from one to another point in this region, and their are almost equal to those found the centre of the scar. All these results show that matter transfer from the cylinder to the sample increases with the number of fretting cycles.

The cylinder used for the fretting tests displays also a scar after the fretting tests. Fig. 6 shows the SEM view of the cylinder scar after 3×10^4 cycles in both secondary and backscattered electrons. This latter one shows clear areas corresponding to the standard composition of 100Cr6 steel, and dark areas where the content of oxygen is close to 50 at%. Traces of titanium, below 0.5 at%, were found in these areas. Thus, the transfer of matter from the sample to the cylinder is negligible.

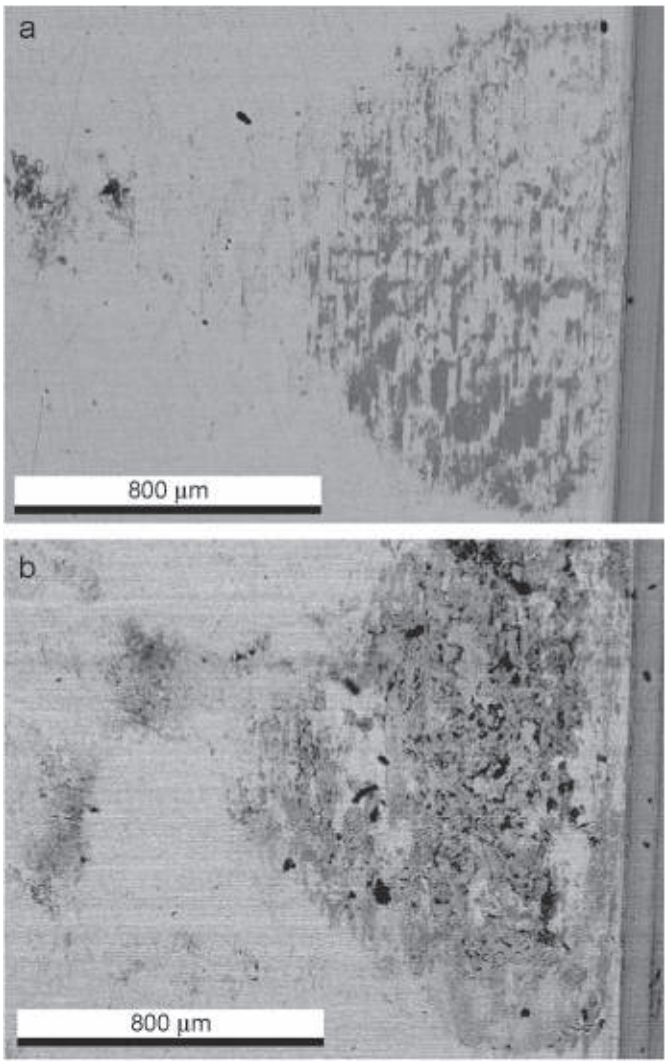

Fig. 6. SEM top views of the fretting cylinder contact area after 3×10^4 fretting cycles: (a) secondary electron image, and (b) backscattering electron image.

3.3. Raman spectroscopy results

The Raman spectra obtained for the laser treated Ti plates before fretting tests are shown in Fig. 7. The relative intensity of the different Raman bands depends on the analysed area, as it was reported in [13]. The bands at 142, 195, 400, 529 and 639 cm^{-1} can be assigned to the anatase TiO_2 phase [20,21], while those placed at 235, 450 and 610 cm^{-1} correspond to the rutile TiO_2 phase [20]. Moreover, we observe a broad band in the 150–350 cm^{-1} range, which can be associated to other titanium oxides or oxinitrides [9,13]. This band is mainly observed in the grooves, while the anatase bands dominate the spectra in the crests between two adjacent grooves. No bands attributed to Magneli phases could be observed.

In the fretting areas, the Raman spectra (Fig. 8) display almost no contribution from titanium oxides. Two different spectra can be associated to two kind of regions clearly differentiated in the optical view of the scars: clear and smooth regions in the centre of the scar, and orange-brown rough regions mainly in the periphery of the scar. For the first ones, the spectrum is dominated by a band

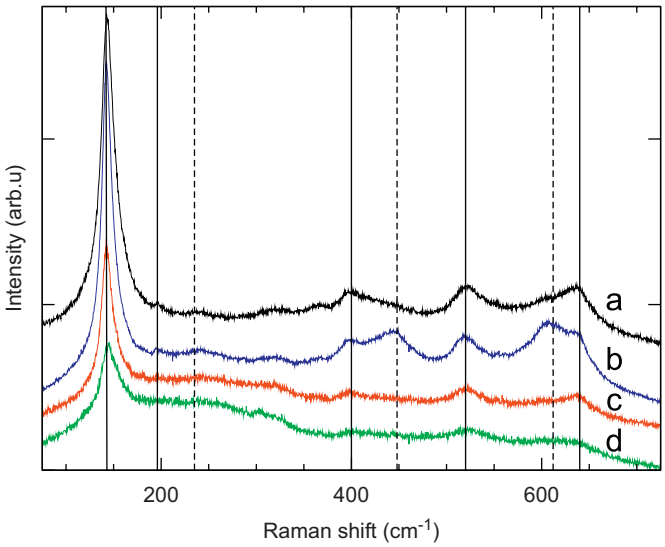

Fig. 7. Raman spectra obtained at different points of the Ti laser treated surface before fretting tests: (a,b) crests between two adjacent grooves, and (c,d) grooves. Continuous and dashed vertical lines indicate the position of the Raman modes of anatase and rutile TiO_2 phases, respectively.

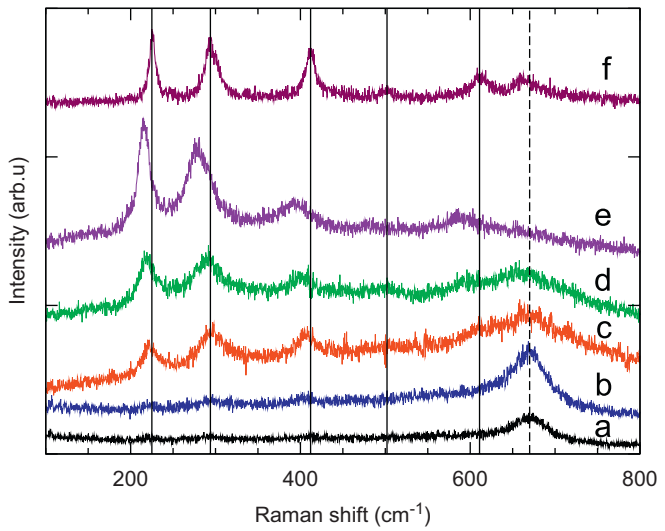

Fig. 8. Raman spectra recorded in two different regions of the scar formed after 3×10^4 fretting cycles in a laser treated Ti plate. (a,b) Smooth region in the center of the scar, laser power: 4 and 40 μW, respectively; (c–f) orange-brown rough region in the periphery of the scar, laser power: 4, 40 μW, 1 mW and 4 μW (after acquisition of spectrum (e)), respectively.

at about 670 cm^{-1}, with very low intensity bands in the 200–600 cm^{-1} range. This spectrum agrees with that reported for the magnetite Fe_3O_4 phase [22,23]. The strong content of iron in the scars revealed by EDS analysis supports this interpretation. The Raman spectrum of magnetite is reported to be very sensitive to the laser power focused on the sample [22–24], due to the transformation of magnetite into hematite α-Fe_2O_3. Thus, two spectra were recorded in the same focusing area: the first one with a very low laser power, about 4 μW, and the second one with a laser power about 40 μW. No significant changes were observed, thus we can neglect heating effects in the spectra (a) and (b) given in Fig. 8.

For the orange-brown rough regions mainly in the periphery of the scar, the band at about 670 cm^{-1} is broadened and three main bands appear at 222, 294, and 406 cm^{-1}, which points to the formation of hematite α-Fe_2O_3. However, these bands are broadened and slightly shifted compared to those reported for the hematite α-Fe_2O_3 [22,23]. Moreover, the intensity and the position of these bands was sensitive to the laser power focused on the sample. Spectra (c), (d) and (e) in Fig. 8 were obtained in the same area with increasing laser power values: 4, 40 μW and 1 mW, respectively. The increase of the laser power induces the shift of these bands to lower wavenumbers and the increase of their intensity. These effects can be explained as due to the heating of the sample by the laser. In fact, heating induces irreversible changes in the Raman spectrum, as is shown in spectrum (f), recorded in the same spot with the lowest laser power (4 μW). The Raman bands are narrower than those in spectrum (c), and the Raman shift values (225, 294, 412, 502 and 611 cm^{-1}) are in good agreement with those reported for the hematite phase α-Fe_2O_3 [22,23]. These results can be explained by the formation of poorly crystallized hematite α-Fe_2O_3, including great amounts of defects, during the fretting process. The heating induced by laser powers about 40 μW leads to a better crystallization of this phase.

The fretting scar in the cylinder was also analysed by micro-Raman spectroscopy. Spectra show the formation of iron oxides, but no signal associated to titanium oxides was found, which is in agreement with EDS results.

4. Discussion

Fretting results show that the contact works in a mixed slip regime for the laser treated Ti plates. Three stages can be distinguished in the fretting process as a function of the number of cycles.

(1) For $N < 5 \times 10^3$ cycles, the contact couple works only in gross slip regime. The interaction of the contact surfaces is weak and it is mainly conducted by mechanics. This is the usual situation at the beginning of the fretting process (low N). Almost no third body particles are present in the contact at this stage of the fretting process.

(2) For 5×10^3 cycles $< N < 1.2 \times 10^4$ cycles, the contact changes from gross slip to partial slip regime. EDX and Raman results show the transfer of iron from the cylinder to the sample surface. Iron is found in the centre of the fretting scars, but it is almost absent in the periphery. The increase of Fe concentration is first observed in the highest points of the rough periphery, corresponding to clusters of matter with a high iron content. By increasing the number of cycles, the iron content increases also in the lowest points. The fretting contact is modified by the increasing presence of particles coming from the cylinder.

(3) For $N > 1.2 \times 10^4$ cycles, the contact couple works in a partial slip regime. The transfer of matter from the cylinder to the sample leads at this stage to the homogenization of the iron content in the fretting scar. Raman spectra show the presence of mainly magnetite Fe_3O_4 phase in the centre of the scar, while magnetite with poorly crystallized hematite α-Fe_2O_3 is found in the periphery of the scar. The contact between the first bodies is carried out mainly through the third body. The variation of nature and the composition of this latter one induces the oscillations of criterion A observed in Fig. 4.

5. Conclusions

The formation of a thick oxidized layer at the surface of pure Ti (CP-Ti grade 4) plates by a laser treatment with a Nd:YAG pulsed

laser was found to improve the fretting properties of titanium plates by reducing the fretting coefficient μ.

The evolution of the energy criterion, A, as a function of the number of fretting cycles revealed a different behaviour of the laser treated samples with respect to the Ti reference. For this latter one, the contact couple works in gross slip regime up to the highest number of fretting cycles in this work, $N = 3 \times 10^4$ cycles. For the laser treated samples, the slip regime changes from gross to partial slip in the 5×10^3 to 1.2×10^4 cycle range.

The analysis of the fretting scars by EDS and micro-Raman spectroscopy revealed the increasing transfer of matter from the cylinder to the sample by increasing the number of fretting cycles in the mixed regime range. This process leads to the homogenization of the iron content in the fretting scar for $N > 1.2 \times 10^4$ cycles. Thus, the contact between the first bodies is carried out mainly through the third body.

Acknowledgements

This work has been financially supported by the Conseil Regional de Bourgogne. The authors thank R. Trigon (PLCB) and Prof. B. Villechaise (LMS—IUT Angoulème, France) as well as D.M. Murray (University of British Columbia, Okanagan) for their help in different parts of this work.

References

[1] Krishna DSR, Brama YL, Sun Y. Thick rutile layer on titanium for tribological applications. Tribol Int 2007;40:329–34.
[2] Dong H, Bell T. Enhanced wear resistance of titanium surfaces by a new thermal oxidation treatment. Wear 2000;238:131–7.
[3] Langlade C, Vannes B, Sarnett T, Autric M. Characterisation of titanium oxide films with Magneli structure elaborated by a sol–gel route. Appl Surf Sci 2002;186:145–9.
[4] Gardos MN, Hong HS, Winer WO. The effect of anion vacancies on the tribological properties of rutile (TiO_{2-x}). Part II. Experimental evidence. Tribol Trans 1990;22(2):209–20.
[5] Akhadejdamrong T, Aiwaza T, Yoshitake M, Mitsuo A, Yamamoto T, Ikuhara Y. Self-lubrication mechanism of chlorine implanted TiN coatings. Wear 2003; 254:668–79.
[6] Aiwaza T, Akhadejdamrong T, Yoshitake M, Mitsuo A. Self-lubrication of nitride ceramic coating by the chloride ion implantation. Surf Coat Technol 2004;177–178:573–81.
[7] Storz O, Gasthuber H, Woydt M. Tribological properties of thermal-sprayed Magneli-type coatings with different stoichiometries Ti_nO_{2n-1}. Surf Coat Technol 2001;140:76–81.
[8] Woydt M. Tribological characteristics of polycrystalline Magneli-type titanium dioxides. Tribol Lett 2000;8:117–30.
[9] Perez del Pino A, Serra P, Morenza JL. Coloring of titanium by pulsed laser processing in air. Thin Solid Films 2002;415:201–5.
[10] Langlade C, Vannes AB, Kraft JM, Martin JR. Surface modification and tribological behaviour of titanium and titanium alloys after YAG-laser treatments. Surf Coat Technol 1998;100/101:383–6.
[11] Le Mercier T, Mariot JM, Goubard F, Quarton M, Fontaine MF, Hague CF. Structural and chemical transformations induced by laser impact on TiO_2 and Nb_2O_5. J Phys Chem Solids 1997;58:679–84.
[12] Lavisse L, Grevey D, Langlade C. The early stage of the laser-induced oxidation of titanium substrates. Appl Surf Sci 2002;18:150–5.
[13] Lavisse L, Jouvard JM, Imhoff L, Heintz O, Korntheuer J, Langlade C, et al. Pulsed laser growth and characterization of thin films on titanium substrates. Appl Surf Sci 2007;253:8226–30.
[14] Han A, Pillon G, Nichici A, Vannes B, Grevey D. Study and evaluation of fretting critical slip conditions by applying the design of experiments method. Wear 2006;261:1080–6.
[15] Vincent L, Berthier Y, Dubourg M. Mechanics and materials in fretting. New York: Elsevier, Sequoia; 1992.
[16] Fouvry S, Vincent L, Kapsa P. Quantification of fretting damage. Wear 1996;200:186–205.
[17] Dubourg MC, Chateauminois A, Villechaise B. In situ analysis and modeling of crack initiation and propagation within model fretting contacts using polymer materials. Tribol Int 2003;36:109–19.
[18] Fouvry S. Analysis of sliding behaviour for fretting loadings: determination of transition criteria. New York: Elsevier, Sequoia; 1994.
[19] Fouvry S. Etude quantitative des degradations en fretting. PhD thesis, No. 97-04, Ecole Centrale de Lyon, 1997.
[20] Moret MP, Zallen R, Vijay DP, Desu SB. Brookite-rich titania films made by pulsed laser deposition. Thin Solid Films 2000;366:8–10.
[21] Ohsaka T, Izumi F, Fujiki Y. Raman spectrum of anatase TiO_2. J Raman Spectrosc 1978;7:321–4.
[22] de Faria DLA, Silva SV, de Oliveira MT. Raman microspectroscopy of some iron oxides and oxyhydroxides. J Raman Spectrosc 1997;28:873.
[23] Bersani D, Lottici PP, Montenero A. Micro-Raman investigation of iron oxide films and powders produced by sol–gel syntheses. J Raman Spectrosc 1999;30:355–60.
[24] Shebanova ON, Lazor P. Raman study of magnetite thermal effects and oxidation. J Raman Spectrosc 2003;34:845–52.